Published in final edited form as:
Cell Stem Cell. 2010 September 3; 7(3): 380–390. doi:10.1016/j.stem.2010.07.011.

The Distinct Metabolic Profile of Hematopoietic Stem Cells Reflects Their Location in a Hypoxic Niche

Tugba Simsek[1,5], **Fatih Kocabas**[1,5], **Junke Zheng**[2,5], **Ralph J. DeBerardinis**[3], **Ahmed I. Mahmoud**[1], **Eric N. Olson**[4], **Jay W. Schneider**[1], **Cheng Cheng Zhang**[2,*], and **Hesham A. Sadek**[1,*]

[1]Department of Internal Medicine, Division of Cardiology

[2]Departments of Physiology and Developmental Biology

[3]Departments of Pediatrics and Genetics

[4]Department of Molecular Biology UT Southwestern Medical Center, Dallas, TX 75390, USA

[5]These authors contributed equally to this work

SUMMARY

Bone marrow transplantation is the primary therapy for numerous hematopoietic disorders. The efficiency of bone marrow transplantation depends on the function of long-term hematopoietic stem cells (LT-HSCs), which is markedly influenced by their hypoxic niche. Survival in this low-oxygen microenvironment requires significant metabolic adaptation. Here, we show that LT-HSCs utilize glycolysis instead of mitochondrial oxidative phosphorylation to meet their energy demands. We used flow cytometry to identify a unique low mitochondrial activity/glycolysis-dependent subpopulation that houses the majority of hematopoietic progenitors and LT-HSCs. Finally, we demonstrate that Meis1 and Hif-1α are markedly enriched in LT-HSCs and that Meis1 regulates HSC metabolism through transcriptional activation of *Hif-1α*. These findings reveal an important transcriptional network that regulates HSC metabolism.

INTRODUCTION

The microenvironment, or niche, plays a crucial role in selfrenewal and differentiation of hematopoietic stem cells (HSCs) (Fuchs et al., 2004; Spradling et al., 2001). One of the hallmarks of the HSC niche is its low-oxygen tension, hence the term “hypoxic niche” (Chow et al., 2001a; Parmar et al., 2007). This low-oxygen environment is not only tolerated by HSCs, but also appears to be essential for their function (Bradley et al., 1978; Chow et al., 2001a; Cipolleschi et al., 1993; Danet et al., 2003; Eliasson and Jönsson, 2010; Katahira and Mizoguchi, 1987; Koller et al., 1992; Kubota et al., 2008; LaIuppa et al., 1998; Lo Celso

*Correspondence: alec.zhang@utsouthwestern.edu (C.C.Z.), hesham.sadek@utsouthwestestern.edu (H.A.S.).

SUPPLEMENTAL INFORMATION

Supplemental Information includes Supplemental Experimental Procedures and two figures and can be found with this article online at doi:10.1016/j.stem.2010.07.011.

et al., 2009; Parmar et al., 2007). The mechanism of this hypoxic tolerance of HSCs, while poorly understood, requires significant metabolic adaptation.

Hif-1 is a master regulator of metabolism. It regulates both glycolysis and mitochondrial respiration, inducing a metabolic shift toward anaerobic glycolysis (Hägg and Wennström, 2005; Kim et al., 2006b; Marín-Hernández et al., 2009; Maxwell et al., 2007; Papandreou et al., 2006; Wang et al., 1995; Zhang et al., 2007). Hif-1 function is dependent on dimerization of the constitutively active Hif-1β subunit and the tightly regulated Hif-1α subunit. Hif-1α undergoes hydroxylation, followed by ubiquitination and degradation during normoxia in most cells (Ivan et al., 2001; Jaakkola et al., 2001; Kamura et al., 2000; Maxwell et al., 1999; Salceda and Caro, 1997). Upregulation of Hif-1α can occur either by transcriptional activation (Hirota et al., 2004; Laughner et al., 2001) or protein stabilization (Li et al., 2005; Nakayama et al., 2004; Qi et al., 2008; Semenza, 2007). Several studies have demonstrated that Hif-1α may play a crucial role in HSCs (Iyer et al., 1998; Ryan et al., 1998) (Kim et al., 2006a); however, the function and mechanism of regulation of Hif-1α in HSCs remain largely unknown.

Meis1 belongs to the Hox family of homeobox genes, which is an evolutionarily conserved set of genes that encode DNA-binding transcription factors (Krumlauf, 1994). Meis1 is expressed in the most primitive hematopoietic populations and is downregulated upon differentiation (Argiropoulos et al., 2007; Imamura et al., 2002; Pineault et al., 2002). Moreover, targeted *Meis1* knockout causes lethality by embryonic day 14.5 with multiple hematopoietic and vascular defects (Azcoitia et al., 2005; Hisa et al., 2004; Imamura et al., 2002). Despite the clear association of Meis1 with HSCs, the precise function of Meis1 in HSCs is not well understood.

In the current study, we outline the unique metabolic characteristics of LT-HSCs and we show that separation of bone marrow cells solely based on their metabolic footprint markedly enriches for HSCs. Finally, we demonstrate that Meis1 regulates HSC metabolism through transcriptional activation of *Hif-1α*.

RESULTS

Metabolic Profile of Mouse LT-HSCs

Lin^-, $Sca\text{-}1^+$, $c\text{-}Kit^+$, $CD34^-$, and $Flk2^-$ (LT-HSCs) cells have low rates of mitochondrial respiration (Figure 1A) and low levels of ATP (Figure 1B). Lower rates of mitochondrial respiration can be attributed to lower energy requirements (i.e., quiescence) and/or utilization of glycolysis instead of oxidative phosphorylation. Therefore, we examined the overall glycolytic flux as determined by the rate of glucose-derived ^{13}C lactate production. As shown in Figure 1C, the rate of glucose-derived ^{13}C lactate production was higher in LT-HSCs compared to whole bone marrow when normalized to cellular ATP. This method determines the source of lactate and not only the amount of lactate produced. This is important because cells can produce lactate from the metabolism of glutamine rather than glucose (DeBerardinis et al., 2007).

Next, we determined the metabolic profile of LT-HSCs by flow cytometry. Whole mouse bone marrow underwent lineage depletion, then was concomitantly stained for Sca-1^{+}, c-Kit^{+}, CD34^{-}, and Flk2^{-} surface expression and for mitotracker incorporation. Cells were also assessed for endogenous NADH fluorescence. These techniques allow profiling of cells based on their mitochondrial proton gradient in the case of mitotracker (Poot et al., 1996) and endogenous NADH fluorescence (Chance and Thorell, 1959) as an index of overall mitochondrial respiration (as the majority of cellular NADH is derived from mitochondrial respiration). The majority of LT-HSCs were localized to a well-defined flow cytometry gate, which contained 6%–9% of total bone marrow cells. Cells in this gate were characterized by low mitochondrial potential (MP) (Figures 1D and 1E) and low NADH fluorescence (Figure 2A). This low MP population contained >80% of LT-HSCs (Figure 1F). Lineage characterization of the low MP population demonstrated that LT-HSCs and Lineage^{-}, Sca-1^{+}, c-Kit^{+} (LSK) cells are the only two populations that are largely localized to the low MP gate, whereas all other lineages had mostly high mitochondrial potential (Figure 1F). Moreover, this low MP gate, although markedly enriched in LT-HSCs and LSK cells, contains all other bone marrow lineages (Figure 1G). To exclude the possibility that this low mitotracker profile is secondary to dye efflux, we used Fumitremorgin C (FTC), a specific blocker of the ABCG2 transporter. The ABCG2 transporter is responsible for dye efflux by the side population (SP) stem cells (Goodell et al., 1997; Scharenberg et al., 2002; Zhou et al., 2001). As shown in Figure 1H, FTC had no effect on the percentage of cells in the low MP gate.

Metabolic Characteristics of High and Low MP Cells

We next characterized the metabolic properties of cells in the low MP gate as they compare to cells with high MP. First, we directly correlated endogenous NADH fluorescence with mitotracker fluorescence. NADH fluorescence is an index of mitochondrial oxidative phosphorylation given that oxidative metabolism yields a significantly higher amount of NADH for each molecule of glucose oxidized when compared to glycolysis (eight molecules NADH compared to two molecules, respectively) (Chance and Thorell, 1959). As shown in Figure 2A, high and low mitotracker cells displayed high and low NADH fluorescence cells, respectively. This result is supported by measurement of oxygen consumption, where the high MP cells displayed significantly higher oxygen consumption rates compared to the low MP cells (Figure 2B).

Low MP cells also preferentially utilized glycolysis for their metabolic needs. As shown in Figure 2D, the rate of ^{13}C lactate production was significantly higher in the low MP cells. We further confirmed this finding by using a specific mitochondrial electron transport chain inhibitor. Inhibition of the electron transport chain complex III by antimycin A (AMA) results in NADH accumulation only in cells that rely on mitochondrial respiration for NADH production. We used this principle to evaluate the source of NADH in high and low MP cells. As shown in Figure 2E, only a small percentage of the low MP cells displayed increased NADH after AMA treatment compared to high MP cells, indicating that mitochondrial respiration is not the main source of NADH in low MP cells. Taken together, these results indicate that the low MP cells do not rely on mitochondrial respiration for energy production, but rather on cytoplasmic glycolysis.

Low MP Cells Are Primed for Hypoxia Resistance

We performed a PCR array for hypoxia related gene expression on freshly isolated high and low MP cells. Under normoxic conditions, the low MP cells displayed significant upregulation of numerous hypoxia-inducible genes and regulatory glycolysis genes (Figure 3A) compared to high MP cells. This was further confirmed by upregulation and stabilization of Hif1-α protein (RNA in Figure 3A and Figure S2A available online, and protein in Figures 3B and 3C) in the low MP cells. These results not only provide a mechanistic explanation of the metabolic phenotype of low MP cells but also suggest that the low MP cells are primed for adaptation to low-oxygen environment. This was corroborated by the significantly higher viability of low MP cells following both severe hypoxic and anoxic stresses (Figure 3D).

Collectively, these results indicate that cells in the low MP gate utilize glycolysis instead of mitochondrial respiration for their energy demands. This metabolic phenotype is associated with normoxic upregulation of *Hif-1*α and its downstream target genes.

Stem Cell Characteristics of Metabolically Sorted Cells

Given the unique metabolic characteristics of LT-HSCs cells, we tested whether isolation of bone marrow cells solely based on their metabolism enriches for HSC. After flow cytometric separation of high and low MP cells, we evaluated their gene expression profile with PCR array. Figure 4A demonstrates that low MP cells express higher levels of numerous HSC-associated transcripts.

Furthermore, we utilized in vitro and in vivo hematopoietic progenitor and HSC assays to characterize the stem cell properties of low MP cells. Low and high MP cells were cultured in methocult medium and the colonies were evaluated after 12 days. Low MP cells displayed a much higher colony forming capacity compared to high MP cells (Figure 4B). Further characterization of colony types revealed that the low MP cell produced a higher percentage of CFU-GEMM type (mixed colonies) with lower percentages of BFU-E and CFU-GM colonies compared to high MP cells (Figures 4C–4E), although the low MP population had significantly higher number of all types of colonies. These results indicate that low MP cells are enriched for hematopoietic progenitor cells.

In vivo bone marrow reconstitution studies following lethal irradiation were undertaken to determine the long-term repopulation capacity of low MP cells. Serial analysis of the peripheral blood of the recipient mice demonstrated a significantly higher percentage of engraftment with the low MP cells compared to high MP cells at all time points (Figures 4F and 4G). Moreover, peripheral blood cells were collected and analyzed by flow cytometry with lineage markers to determine the capacity of low MP cells to repopulate different hematopoietic lineages. As shown in Figure S1A, the low MP cells repopulated all tested lymphoid ($CD45.2^+Thy1.2^+$, $CD45.2^+B220^+$) and myeloid lineages ($CD45.2^+Mac\text{-}1^+$, $CD45.2^+Gr\text{-}1^+$). Additional studies were undertaken in which the bone marrow was depleted of HSCs by flow cytometric separation of LSK cells, followed by equal distribution of LSK cells to the high and low MP populations. Bone marrow reconstitution studies using these high and low MP populations with equal numbers of HSCs demonstrated no difference in

transplantation efficiency (Figure S1B). This confirms that the enhanced reconstitution capacity by the low MP population is due to localization of LT-HSCs to the low MP gate. Collectively, these results confirm that the low MP cell fraction of the bone marrow is highly enriched in both hematopoietic progenitors and long-term repopulating HSCs.

Expression of Hif-1α in LT-HSCs

In order to determine the mechanism of the glycolytic metabolic phenotype of LT-HSCs, we evaluated the expression pattern of Hif-1α in LT-HSCs and WBM (Figure 5A). WBM and LT-HSCs underwent fixation followed by permeabilization and immunocytochemical staining for Hif-1α. Here, we show that the majority (89%) of LT-HSCs express Hif-1α, whereas less than 30% of the WBM cells are Hif-1α positive. Upregulation of *Hif-1*α mRNA was confirmed by real-time PCR as shown in Figure S2B.

Meis1 Is a Transcriptional Activator of *Hif-1*α

Meis1 is a HSC-associated transcription factor required for definitive hematopiesis; however, its precise role in HSCs is not well understood. We determined that whereas only a small percentage of WBM cells express Meis1 protein (1.4%), the vast majority of LT-HSCs are Meis1 positive (96.2%) (Figure 5B). Moreover, we colocalized Hif-1α and Meis1 proteins by immunocytochemistry and found that the majority of Meis1 positive cells were also positive for Hif-1α (85.2%) (Figure 5C). This expression pattern of Hif-1α and Meis1 remained unchanged hours after isolation of bone marrow cells, indicating that the expression of Hif-1α may not be simply secondary to the in vivo environment in the bone marrow.

These findings led us to examine whether Hif-1α expression by LT-HSCs is downstream of the HSC-associated transcription factor Meis1. We identified an evolutionarily conserved Meis1 consensus binding sequence in the *Hif-1*α first intronic region (Figure 5D). Luciferase assays were carried out with wild-type *Hif-1*α promoter (Hif1-α-pGL2) and a *Hif-1*α promoter harboring a mutated Meis1 binding sequence (mut-TGAC-Hif-1α-pGL2). Increasing concentrations of Meis1 expression vector (CMVM-*Meis1*) resulted in dose-dependent transcriptional activation of *Hif-1*α. This activation was dependent on binding of Meis1 to its consensus binding sequence in the *Hif-1*α first intronic region because mutation of the seed sequence completely abolished the activation of *Hif-1*α by Meis1 (Figure 5E).

To determine whether Meis1 is required for *Hif-1*α expression, we utilized siRNA to knockdown Meis1 in freshly isolated LT-HSCs. Scrambled Meis1 siRNA was used as control. Transfection with Meis1 siRNA resulted in diminution of *Meis1* mRNA levels. This was associated with a marked downregulation of *Hif-1*α mRNA (Figure 5F). Taken together, these results indicate that Meis1 is required for optimal transcriptional activation of *Hif-1*α in LT-HSCs.

To confirm the in vivo binding of Meis1 to its conserved sequence in the *Hif-1*α gene, we performed chromatin immunoprecipitation (ChIP) assays in Kasumi1 cells. The results confirmed that Meis1 binds in vivo to its conserved sequence in the *Hif-1*α first intronic

region as determined by real-time PCR following immunoprecipitation with Meis1 antibody (Figure 5H). PCR products are shown in the right panel.

DISCUSSION

Stem cell separation techniques generally rely on the pattern of expression of specific membrane proteins. As a result, isolation of HSCs requires the combination of several antibodies such that stem cells are defined by the presence or absence of certain epitopes or markers (Challen et al., 2009; Goodell et al., 1996; Kiel et al., 2007; McCune et al., 1988; Murray et al., 1995; Péault et al., 1993). Although several reports have indicated that HSCs are resistant to hypoxia (Cipolleschi et al., 1993) and reside within hypoxic niches in the bone marrow (Chow et al., 2001b; Li and Li, 2006; Parmar et al., 2007), these characteristics have not been exploited for identification of unique metabolic properties of HSCs, or for HSC enrichment.

In the current study, we define the metabolic phenotype of mouse HSCs. We demonstrate that LT-HSCs cells are localized to a distinct population of cells characterized by low mitochondrial potential (low MP). This population represents only 6%–9% of the total bone marrow, but contains >80% of LT-HSCs, determined by surface marker expression. We show that both LT-HSCs and low MP cells have low ATP levels and utilize cytoplasmic glycolysis instead of mitochondrial oxidative phosphorylation. This metabolic phenotype is associated with upregulation of Hif-1α, at both the transcript and the protein levels. Separation of cells solely based on this metabolic profile markedly enriches for HSCs as determined by in vitro colony forming assays and in vivo long-term repopulation assays. Finally, we show that the HSC-associated transcription factor Meis1 regulates HSC metabolism through transcriptional activation of *Hif-1*α.

Hif-1α is a master regulator of metabolism known to regulate various aspects of cellular response to hypoxic stress. Although the mechanism of oxygen-dependent posttranslational regulation of *Hif-1*α is well understood, little is known about its transcriptional regulation. A number of reports indicate that *Hif-1*α is regulated at the transcriptional level both during hypoxia and normoxia (Belaiba et al., 2007; Blouin et al., 2004; Hirota et al., 2004; Jiang et al., 1997; Laughner et al., 2001; Liu et al., 2004). In the current study, we show that Meis1 activates *Hif-1*α transcription in LT-HSCs through binding to its conserved consensus binding sequence in the *Hif-1*α first intronic region.

The metabolic phenotype of HSCs outlined here is supportive of the adaptability of HSCs to the physiologic low-oxygen tension in the bone marrow hypoxic niches. Under these hypoxic conditions, glycolytic metabolism predominates and can provide sufficient amounts of ATP to sustain HSCs. This metabolic phenotype also confers a survival advantage on HSCs during severe hypoxic or anoxic insults that would invariably eliminate differentiated cells that rely on oxidative metabolism. Importantly, the transcriptional regulation of *Hif-1*α by Meis1 highlights the involvement of stem cell-associated transcription factors in regulation of HSC metabolism and indicates that the glycolytic phenotype of HSCs is not merely a product of their hypoxic environment.

EXPERIMENTAL PROCEDURES

LT-HSC Isolation

LT-HSCs were isolated from the bone marrow cells of 4- to 6-month-old C57BL/6 mice by FACS after surface marker staining for Lin, Sca-1, C-Kit, CD34, and Flk2 to identify Lin^-, $Sca\text{-}1^+$ $C\text{-}kit^+$, and $CD34/Flk2^-$ cells (LT-HSCs). All antibodies were purchased from BD PharMingen. In studies where LT-HSCs were isolated for metabolic analysis, magnetic lineage depletion (autoMACS separator, Miltenyibiotec) was utilized. In these studies, additional control fluorescent surface marker staining was performed, and the cells were evaluated by flow cytometry for ensuring that adequate lineage depletion (>95% lineage depletion) was reproducibly achieved. For metabolic studies, LT-HSCs isolated from 62 mice were pooled, and metabolic studies were performed within 24 hr of isolation.

Metabolic Assays

Oxygen consumption was measured with the BD Oxygen Biosensor System in accordance with the manufacturer's recommendations. A total of 2 to 3×10^5 cells/well were used. Oxygen consumption was determined after 2 hr of culture in the biosensor.

ATP levels were quantified with ATP Bioluminescence Assay Kit HS II (Roche) in accordance with the manufacturer's recommendations. A total of 2 to 3×10^5 cells/well were used.

Lactate production was measured with gas chromatography-mass spectrometry. Cells were cultured for 12 hr in a medium supplemented with 10 mM D-[1-^{13}C]-glucose (Cambridge Isotope Labs) to allow up to half of the glucose-derived lactate pool to be labeled on C-3. The samples were analyzed for lactate abundance. The final results are presented as nMoles ^{13}C-Lactate/nMol ATP.

Mitochondrial source of NADH was determined with the electron transport chain complex III inhibitor antimycin A (AMA). AMA leads to cessation of electron flow through the respiratory chain resulting in rapid accumulation of NADH from the Krebs cycle. Stock AMA (Sigma Aldrich) was prepared at 1 M in DMSO. A baseline NADH fluorescence gate was set with untreated high and low MP cells. High and low mitochondrial potential cells were then treated with 2 μM AMA for 5 min and profiled for NADH fluorescence. Cells with mitochondrial source of NADH production display an increase in NADH fluorescence following AMA treatment.

Flow Cytometric Profiling and Separation of Cells Based on Mitochondrial Activity

Flow cytometric profiling and separation of BM cells based on their mitochondrial activity was performed with mitotracker dyes and endogenous NADH fluorescence. The metabolic profile of mouse LT-HSCs was determined with concomitant surface marker and mitotracker staining. Mitotracker dyes that accumulate within mitochondria on the basis of mitochondrial proton gradient (MitoTracker deep red 633, MitoTracker Red CMXRos and MitoTracker Red CM-H2XRos) (Poot et al., 1996), as well as nonproton gradient sensitive dyes (MitoTracker Green), were used. Endogenous NADH fluorescence was measured flow

cytometrically at 37°C with a UV laser (Ex: 350 nm, Em: 460 nm, Moflo analyzer, Cytomation) as described previously (Chance and Thorell, 1959). Flow cytometric separation of high and low MP cells was carried out by separating cells in the low MP gate (6%–9%) and an equivalent number of cells with high mitochondrial potential.

Stem Cell Assays

Colony forming cell (CFC) assays were performed on high and low MP cells separated solely on the basis of the flow cytometric mitochondrial profile according to recommendations (Methocult, Stem Cell Technologies). For in vivo bone marrow reconstitution studies, high and low MP cells were isolated from 8- to 10-week-old C57BL/6 CD45.2 mice. Equal numbers of high and low MP CD45.2 donor cells (5×10^4) were mixed with 5×10^4 freshly isolated CD45.1 competitor bone marrow cells, and the mixture was injected intravenously via the retro-orbital route into each of a group of 6- to 9-week-old CD45.1 mice previously irradiated with a total dose of 10 Gy. For measuring reconstitution of transplanted mice, peripheral blood was collected at the indicated times after transplant and the presence of $CD45.1^+$ and $CD45.2^+$ cells in lymphoid and myeloid compartments were measured as described (Zhang and Lodish, 2004, 2005). Separate studies were performed were LSK cells were depleted from the bone marrow by flow cytometry, followed by equal distribution of LSK cells to high and low MP populations (1500 LSK cells per group). CD45.2 high and low MP donor cells (5×10^4) were mixed with 5×10^4 freshly isolated CD45.1 competitor bone marrow cells.

Gene Profile of Low and High MP Cells

RNA was extracted from high and low MP cells by using TRIzol (Invitrogen) in accordance with the manufacturer's instructions. cDNA was retrotranscribed with an RT-PCR kit (SA Biosciences). Mouse Real-Time Syber Green PCR Mix was purchased from SuperArray. PCR was performed on an ABI Prism 7700 Sequence Detector (Applied Biosystems). HSCs and hypoxia primer sets (SABiosciences) were used. The data were analyzed with the DDCt method. Fold change was calculated as difference in gene expression between high and low MP cells. Additional real-time PCR for *Meis1*, *Hif-1*α was performed with the SyberGreen method (Applied Biosystems) on ABI Prism 7700 Sequence Detector (Applied Biosystems) and primers specific for the selected genes.

Intracellular Detection of Hif-1α and Meis1 Proteins

Hif-1α by Meis1 proteins were detected by immunocytochemistry as follows; fresh bone marrow cells underwent fixation with 4% paraformaldehyde for 10 min at room temperature. After permeabilization (0.01% Triton) and serum block, cells were incubated overnight with primary antibodies (1:50 dilution anti-Hif-1α and 1:50 dilution anti-Meis1). Staining was assessed by flow cytometry after incubation with corresponding fluorophore-conjugated secondary antibody.

Transcriptional Activation of *Hif-1α* by Meis1

Luciferase reporter assay was performed with an 818 bp long DNA fragment from the first intronic region of *Hif-1*α containing the conserved Meis1 binding site (+1799 bp from ATG

start site, chr14:61,232,973–61,233,790) was amplified from mouse genomic DNA and used for generation of TGAC-Hif-1α-pGL2 and mut-TGAC-Hif-1α-pGL2 reporter vectors. Transcriptional activation of *Hif-1*α by Meis1 was evaluated with Hif-1α-pGL2 and mut-TGAC-Hif-1αpGL2 vectors.

Meis1 siRNA knockdown was carried out in freshly isolated LT-HSCs (4×10^4 cells/reaction). Cells were transfected with 50 nM of Silencer Select Custom-designed siRNA corresponding to Meis1 (#s237712), and nontargeting control siRNA (Silencer Select Negative Control #1 siRNA, Applied Biosystems). Transfections were performed with the Amaxa Nucleofector device (program Y-001) with Amaxa $CD34^+$ Cell Nucleofector Kit (Lonza Cologne AG) in accordance with the manufacturer's instructions. After incubation at 37°C for 20 hr, transfected LT-HSCs cells were harvested and analyzed by real-time PCR with *Meis1* and *Hif-1*α primers.

ChIP assay was performed to evaluate the in vivo binding of Meis1 to its consensus sequence in the *Hif-1*α enhancer region. The assays were done using the ChIP kit (Upstate, cat#17–295) according to the manufacturer's instructions. Meis1 polyclonal antibody (Santa Cruz, cat# sc-10599) was utilized.

Statistical Analysis

Significance levels were calculated with a Student's t test.

Supplementary Material

Refer to Web version on PubMed Central for supplementary material.

Acknowledgments

We thank Dr. Joseph Garcia for his valuable input and Sean Goetsch for technical assistance. Work in the laboratory of H.A.S. was supported by grants from the American Heart Association and the Donald W. Reynolds Center for Clinical Cardiovascular Research. Support for C.C.Z. was provided by the Welch Foundation (I-1701).

REFERENCES

Argiropoulos B, Yung E, Humphries RK. Unraveling the crucial roles of Meis1 in leukemogenesis and normal hematopoiesis. Genes Dev. 2007; 21:2845–2849. [PubMed: 18006680]

Azcoitia V, Aracil M, Martínez-A C, Torres M. The homeodomain protein Meis1 is essential for definitive hematopoiesis and vascular patterning in the mouse embryo. Dev. Biol. 2005; 280:307–320. [PubMed: 15882575]

Belaiba RS, Bonello S, Zähringer C, Schmidt S, Hess J, Kietzmann T, Görlach A. Hypoxia up-regulates hypoxia-inducible factor-1alpha transcription by involving phosphatidylinositol 3-kinase and nuclear factor kappaB in pulmonary artery smooth muscle cells. Mol. Biol. Cell. 2007; 18:4691–4697. [PubMed: 17898080]

Blouin CC, Pagé EL, Soucy GM, Richard DE. Hypoxic gene activation by lipopolysaccharide in macrophages: Implication of hypoxia-inducible factor 1alpha. Blood. 2004; 103:1124–1130. [PubMed: 14525767]

Bradley TR, Hodgson GS, Rosendaal M. The effect of oxygen tension on haemopoietic and fibroblast cell proliferation in vitro. J. Cell. Physiol. 1978; 97 Suppl 1(3 Pt 2):517–522. [PubMed: 730784]

Challen GA, Boles N, Lin KK, Goodell MA. Mouse hematopoietic stem cell identification and analysis. Cytometry A. 2009; 75:14–24. [PubMed: 19023891]

Chance B, Thorell B. Localization and kinetics of reduced pyridine nucleotide in living cells by microfluorometry. J. Biol. Chem. 1959; 234:3044–3050. [PubMed: 13809109]

Chow DC, Wenning LA, Miller WM, Papoutsakis ET. Modeling pO(2) distributions in the bone marrow hematopoietic compartment. I. Krogh's model. Biophys. J. 2001a; 81:675–684. [PubMed: 11463616]

Chow DC, Wenning LA, Miller WM, Papoutsakis ET. Modeling pO(2) distributions in the bone marrow hematopoietic compartment. II. Modified Kroghian models. Biophys. J. 2001b; 81:685–696. [PubMed: 11463617]

Cipolleschi MG, Dello Sbarba P, Olivotto M. The role of hypoxia in the maintenance of hematopoietic stem cells. Blood. 1993; 82:2031–2037. [PubMed: 8104535]

Danet GH, Pan Y, Luongo JL, Bonnet DA, Simon MC. Expansion of human SCID-repopulating cells under hypoxic conditions. J. Clin. Invest. 2003; 112:126–135. [PubMed: 12840067]

DeBerardinis RJ, Mancuso A, Daikhin E, Nissim I, Yudkoff M, Wehrli S, Thompson CB. Beyond aerobic glycolysis: Transformed cells can engage in glutamine metabolism that exceeds the requirement for protein and nucleotide synthesis. Proc. Natl. Acad. Sci. USA. 2007; 104:19345–19350. [PubMed: 18032601]

Eliasson P, Jönsson JI. The hematopoietic stem cell niche: Low in oxygen but a nice place to be. J. Cell. Physiol. 2010; 222:17–22. [PubMed: 19725055]

Fuchs E, Tumbar T, Guasch G. Socializing with the neighbors: Stem cells and their niche. Cell. 2004; 116:769–778. [PubMed: 15035980]

Goodell MA, Brose K, Paradis G, Conner AS, Mulligan RC. Isolation and functional properties of murine hematopoietic stem cells that are replicating in vivo. J. Exp. Med. 1996; 183:1797–1806. [PubMed: 8666936]

Goodell MA, Rosenzweig M, Kim H, Marks DF, DeMaria M, Paradis G, Grupp SA, Sieff CA, Mulligan RC, Johnson RP. Dye efflux studies suggest that hematopoietic stem cells expressing low or undetectable levels of CD34 antigen exist in multiple species. Nat. Med. 1997; 3:1337–1345. [PubMed: 9396603]

Hägg M, Wennström S. Activation of hypoxia-induced transcription in normoxia. Exp. Cell Res. 2005; 306:180–191. [PubMed: 15878343]

Hirota K, Fukuda R, Takabuchi S, Kizaka-Kondoh S, Adachi T, Fukuda K, Semenza GL. Induction of hypoxia-inducible factor 1 activity by muscarinic acetylcholine receptor signaling. J. Biol. Chem. 2004; 279:41521–41528. [PubMed: 15280370]

Hisa T, Spence SE, Rachel RA, Fujita M, Nakamura T, Ward JM, Devor-Henneman DE, Saiki Y, Kutsuna H, Tessarollo L, et al. Hematopoietic, angiogenic and eye defects in Meis1 mutant animals. EMBO J. 2004; 23:450–459. [PubMed: 14713950]

Imamura T, Morimoto A, Takanashi M, Hibi S, Sugimoto T, Ishii E, Imashuku S. Frequent co-expression of HoxA9 and Meis1 genes in infant acute lymphoblastic leukaemia with MLL rearrangement. Br. J. Haematol. 2002; 119:119–121. [PubMed: 12358913]

Ivan M, Kondo K, Yang H, Kim W, Valiando J, Ohh M, Salic A, Asara JM, Lane WS, Kaelin WG Jr. HIFalpha targeted for VHL-mediated destruction by proline hydroxylation: implications for O2 sensing. Science. 2001; 292:464–468. [PubMed: 11292862]

Iyer NV, Kotch LE, Agani F, Leung SW, Laughner E, Wenger RH, Gassmann M, Gearhart JD, Lawler AM, Yu AY, Semenza GL. Cellular and developmental control of O2 homeostasis by hypoxia-inducible factor 1 alpha. Genes Dev. 1998; 12:149–162. [PubMed: 9436976]

Jaakkola P, Mole DR, Tian YM, Wilson MI, Gielbert J, Gaskell SJ, Kriegsheim Av, Hebestreit HF, Mukherji M, Schofield CJ, et al. Targeting of HIF-alpha to the von Hippel-Lindau ubiquitylation complex by O2-regulated prolyl hydroxylation. Science. 2001; 292:468–472. [PubMed: 11292861]

Jiang BH, Agani F, Passaniti A, Semenza GL. V-SRC induces expression of hypoxia-inducible factor 1 (HIF-1) and transcription of genes encoding vascular endothelial growth factor and enolase 1: involvement of HIF-1 in tumor progression. Cancer Res. 1997; 57:5328–5335. [PubMed: 9393757]

Kamura T, Sato S, Iwai K, Czyzyk-Krzeska M, Conaway RC, Conaway JW. Activation of HIF1alpha ubiquitination by a reconstituted von Hippel-Lindau (VHL) tumor suppressor complex. Proc. Natl. Acad. Sci. USA. 2000; 97:10430–10435. [PubMed: 10973499]

Katahira J, Mizoguchi H. Improvement of culture conditions for human megakaryocytic and pluripotent progenitor cells by low oxygen tension. Int. J. Cell Cloning. 1987; 5:412–420. [PubMed: 3624921]

Kiel MJ, Radice GL, Morrison SJ. Lack of evidence that hematopoietic stem cells depend on N-cadherin-mediated adhesion to osteoblasts for their maintenance. Cell Stem Cell. 2007; 1:204–217. [PubMed: 18371351]

Kim CG, Lee JJ, Jung DY, Jeon J, Heo HS, Kang HC, Shin JH, Cho YS, Cha KJ, Kim CG, et al. Profiling of differentially expressed genes in human stem cells by cDNA microarray. Mol. Cells. 2006a; 21:343–355. [PubMed: 16819296]

Kim JW, Tchernyshyov I, Semenza GL, Dang CV. HIF-1-mediated expression of pyruvate dehydrogenase kinase: a metabolic switch required for cellular adaptation to hypoxia. Cell Metab. 2006b; 3:177–185. [PubMed: 16517405]

Koller MR, Bender JG, Miller WM, Papoutsakis ET. Reduced oxygen tension increases hematopoiesis in long-term culture of human stem and progenitor cells from cord blood and bone marrow. Exp. Hematol. 1992; 20:264–270. [PubMed: 1544397]

Krumlauf R. Hox genes in vertebrate development. Cell. 1994; 78:191–201. [PubMed: 7913880]

Kubota Y, Takubo K, Suda T. Bone marrow long label-retaining cells reside in the sinusoidal hypoxic niche. Biochem. Biophys. Res. Commun. 2008; 366:335–339. [PubMed: 18047833]

LaIuppa JA, Papoutsakis ET, Miller WM. Oxygen tension alters the effects of cytokines on the megakaryocyte, erythrocyte, and granulocyte lineages. Exp. Hematol. 1998; 26:835–843. [PubMed: 9694504]

Laughner E, Taghavi P, Chiles K, Mahon PC, Semenza GL. HER2 (neu) signaling increases the rate of hypoxia-inducible factor 1alpha (HIF-1alpha) synthesis: novel mechanism for HIF-1-mediated vascular endothelial growth factor expression. Mol. Cell. Biol. 2001; 21:3995–4004. [PubMed: 11359907]

Li Z, Li L. Understanding hematopoietic stem-cell microenvironments. Trends Biochem. Sci. 2006; 31:589–595. [PubMed: 16911868]

Li Z, Wang D, Messing EM, Wu G. VHL protein-interacting deubiquitinating enzyme 2 deubiquitinates and stabilizes HIF-1alpha. EMBO Rep. 2005; 6:373–378. [PubMed: 15776016]

Liu Q, Möller U, Flügel D, Kietzmann T. Induction of plasminogen activator inhibitor I gene expression by intracellular calcium via hypoxia-inducible factor-1. Blood. 2004; 104:3993–4001. [PubMed: 15328163]

Lo Celso C, Wu JW, Lin CP. In vivo imaging of hematopoietic stem cells and their microenvironment. J Biophotonics. 2009; 2:619–631. [PubMed: 19847800]

Marín-Hernández A, Gallardo-Pérez JC, Ralph SJ, Rodríguez-Enríquez S, Moreno-Sánchez R. HIF-1alpha modulates energy metabolism in cancer cells by inducing over-expression of specific glycolytic isoforms. Mini Rev. Med. Chem. 2009; 9:1084–1101. [PubMed: 19689405]

Maxwell PH, Wiesener MS, Chang GW, Clifford SC, Vaux EC, Cockman ME, Wykoff CC, Pugh CW, Maher ER, Ratcliffe PJ. The tumour suppressor protein VHL targets hypoxia-inducible factors for oxygen-dependent proteolysis. Nature. 1999; 399:271–275. [PubMed: 10353251]

Maxwell PJ, Gallagher R, Seaton A, Wilson C, Scullin P, Pettigrew J, Stratford IJ, Williams KJ, Johnston PG, Waugh DJ. HIF-1 and NF-kappaB-mediated upregulation of CXCR1 and CXCR2 expression promotes cell survival in hypoxic prostate cancer cells. Oncogene. 2007; 26:7333–7345. [PubMed: 17533374]

McCune JM, Namikawa R, Kaneshima H, Shultz LD, Lieberman M, Weissman IL. The SCID-hu mouse: Murine model for the analysis of human hematolymphoid differentiation and function. Science. 1988; 241:1632–1639. [PubMed: 2971269]

Murray L, Chen B, Galy A, Chen S, Tushinski R, Uchida N, Negrin R, Tricot G, Jagannath S, Vesole D, et al. Enrichment of human hematopoietic stem cell activity in the CD34+Thy-1+Lin- subpopulation from mobilized peripheral blood. Blood. 1995; 85:368–378. [PubMed: 7529060]

Nakayama K, Frew IJ, Hagensen M, Skals M, Habelhah H, Bhoumik A, Kadoya T, Erdjument-Bromage H, Tempst P, Frappell PB, et al. Siah2 regulates stability of prolyl-hydroxylases, controls HIF1alpha abundance, and modulates physiological responses to hypoxia. Cell. 2004; 117:941–952. [PubMed: 15210114]

Papandreou I, Cairns RA, Fontana L, Lim AL, Denko NC. HIF-1 mediates adaptation to hypoxia by actively downregulating mitochondrial oxygen consumption. Cell Metab. 2006; 3:187–197. [PubMed: 16517406]

Parmar K, Mauch P, Vergilio JA, Sackstein R, Down JD. Distribution of hematopoietic stem cells in the bone marrow according to regional hypoxia. Proc. Natl. Acad. Sci. USA. 2007; 104:5431–5436. [PubMed: 17374716]

Péault B, Weissman I, Baum C. Analysis of candidate human blood stem cells in “humanized” immune-deficiency SCID mice. Leukemia. 1993; 7(Suppl 2):S98–S101. [PubMed: 7689676]

Pineault N, Helgason CD, Lawrence HJ, Humphries RK. Differential expression of Hox, Meis1, and Pbx1 genes in primitive cells throughout murine hematopoietic ontogeny. Exp. Hematol. 2002; 30:49–57. [PubMed: 11823037]

Poot M, Zhang YZ, Krämer JA, Wells KS, Jones LJ, Hanzel DK, Lugade AG, Singer VL, Haugland RP. Analysis of mitochondrial morphology and function with novel fixable fluorescent stains. J. Histochem. Cytochem. 1996; 44:1363–1372. [PubMed: 8985128]

Qi J, Nakayama K, Gaitonde S, Goydos JS, Krajewski S, Eroshkin A, Bar-Sagi D, Bowtell D, Ronai Z. The ubiquitin ligase Siah2 regulates tumorigenesis and metastasis by HIF-dependent and -independent pathways. Proc. Natl. Acad. Sci. USA. 2008; 105:16713–16718. [PubMed: 18946040]

Ryan HE, Lo J, Johnson RS. HIF-1 alpha is required for solid tumor formation and embryonic vascularization. EMBO J. 1998; 17:3005–3015. [PubMed: 9606183]

Salceda S, Caro J. Hypoxia-inducible factor 1alpha (HIF-1alpha) protein is rapidly degraded by the ubiquitin-proteasome system under normoxic conditions. Its stabilization by hypoxia depends on redox-induced changes. J. Biol. Chem. 1997; 272:22642–22647. [PubMed: 9278421]

Scharenberg CW, Harkey MA, Torok-Storb B. The ABCG2 transporter is an efficient Hoechst 33342 efflux pump and is preferentially expressed by immature human hematopoietic progenitors. Blood. 2002; 99:507–512. [PubMed: 11781231]

Semenza GL. Hypoxia-inducible factor 1 (HIF-1) pathway. Sci. STKE. 2007; 2007:cm8. [PubMed: 17925579]

Spradling A, Drummond-Barbosa D, Kai T. Stem cells find their niche. Nature. 2001; 414:98–104. [PubMed: 11689954]

Wang GL, Jiang BH, Rue EA, Semenza GL. Hypoxia-inducible factor 1 is a basic-helix-loop-helix-PAS heterodimer regulated by cellular O2 tension. Proc. Natl. Acad. Sci. USA. 1995; 92:5510–5514. [PubMed: 7539918]

Zhang CC, Lodish HF. Insulin-like growth factor 2 expressed in a novel fetal liver cell population is a growth factor for hematopoietic stem cells. Blood. 2004; 103:2513–2521. [PubMed: 14592820]

Zhang CC, Lodish HF. Murine hematopoietic stem cells change their surface phenotype during ex vivo expansion. Blood. 2005; 105:4314–4320. [PubMed: 15701724]

Zhang H, Gao P, Fukuda R, Kumar G, Krishnamachary B, Zeller KI, Dang CV, Semenza GL. HIF-1 inhibits mitochondrial biogenesis and cellular respiration in VHL-deficient renal cell carcinoma by repression of C-MYC activity. Cancer Cell. 2007; 11:407–420. [PubMed: 17482131]

Zhou S, Schuetz JD, Bunting KD, Colapietro AM, Sampath J, Morris JJ, Lagutina I, Grosveld GC, Osawa M, Nakauchi H, Sorrentino BP. The ABC transporter Bcrp1/ABCG2 is expressed in a wide variety of stem cells and is a molecular determinant of the side-population phenotype. Nat. Med. 2001; 7:1028–1034. [PubMed: 11533706]

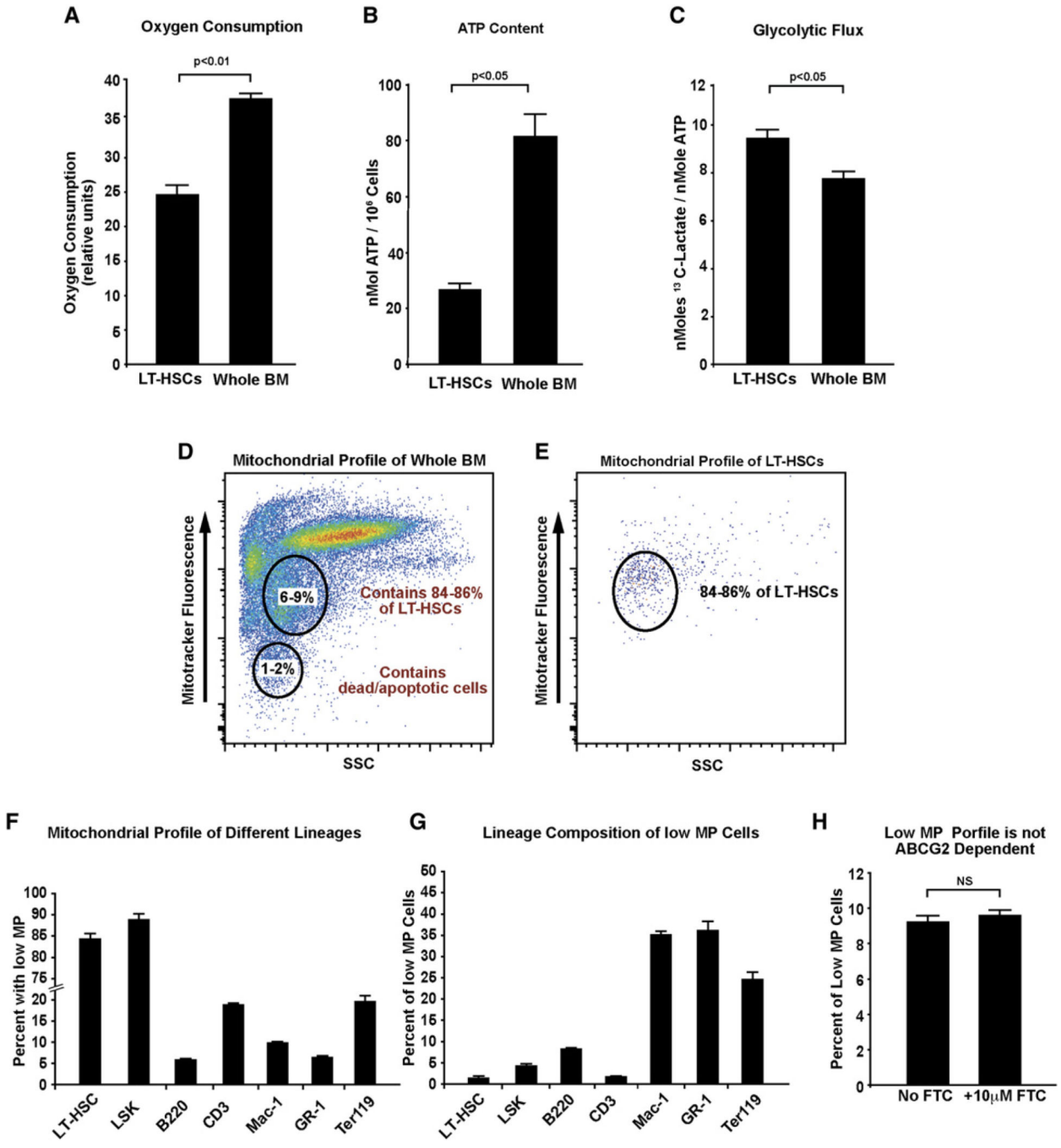

Figure 1. Metabolic Profile of Mouse HSCs

(A) Oxygen consumption of Lin^{-}, SCA-1^{+}, c-Kit^{+}, CD34^{-}, and Flk2^{-} cells (LT-HSCs) and whole bone marrow demonstrating lower rates of oxygen consumption by LT-HSCs (n = 3).

(B) ATP level of LT-HSCs and whole bone marrow demonstrating lower ATP levels in LT-HSCs (n = 3).

(C) Glycolytic flux of LT-HSCs and whole bone marrow demonstrating higher rates of glycolysis in LT-HSCs (n = 3).

(D) Flow cytometry profile of whole mouse bone marrow stained with mitotracker. Note the distinct populations with different mitotracker fluorescence.
(E) Mitotracker profile of LT-HSCs. The majority of LT-HSCs (84%–86%) are localized to a distinct population (6%–9% of total bone marrow cells) with low mitochondrial potential (MP cells).
(F) Mitotracker profile of different bone marrow lineages. Note that whereas the majority of LT-HSCs and LSK cells are localized to the low mitochondrial potential gate, the majority of all other lineages have high mitochondrial potential (n = 4).
(G) Lineage composition of the low MP cells. Note that whereas the low MP gate is markedly enriched in LT-HSCs and LSK cells, it also contains all other bone marrow lineages (n = 4).
(H) Percentage of cells in the low MP gate following pretreatment with FTC (a specific blocker of the ABCG2 transporter). Note that FTC had no effect on the percentage of cells in the low MP gate (n = 3). This indicates that the low MP profile is not secondary to dye efflux. Data presented as mean ± SEM.

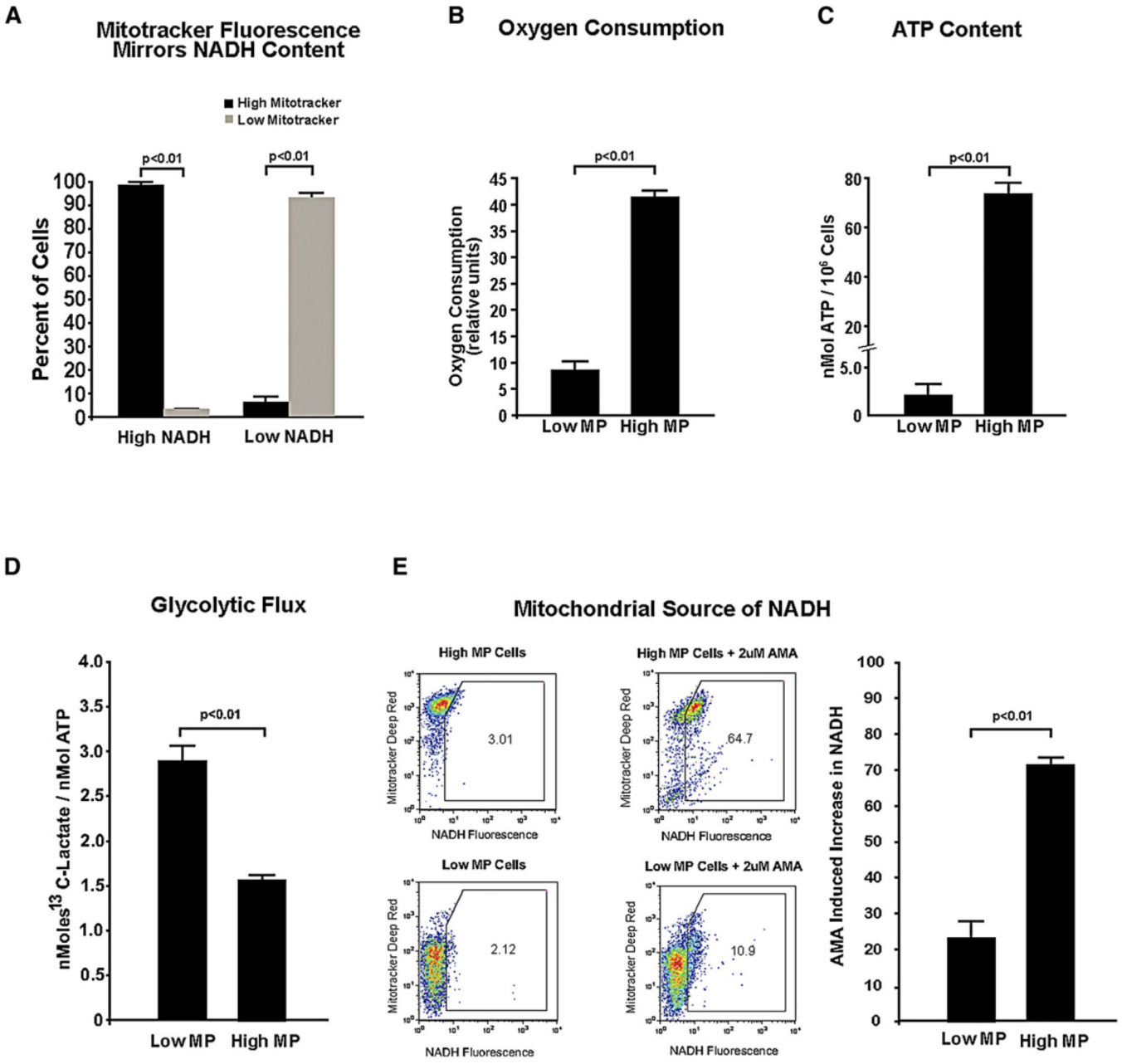

Figure 2. Low MP Cells Are Glycolytic

(A) Comparison between mitotracker fluorescence and endogenous NADH fluorescence of both high MP and low MP cells. Note the direct correlation between mitotracker fluorescence and NADH fluorescence, which provides further proof of the metabolic state of these two populations (n = 4).

(B) Oxygen consumption of high and low MP cells. Note the significantly lower rates oxygen consumption in the low MP cells (n = 3).

(C) ATP content of high and low MP cells demonstrating a significantly lower levels of ATP in the low MP cells (n = 3).

(D) Measurement of glycolytic flux of high and low MP cells as determined by ^{13}C-Lactate production. The low MP cells displayed significantly higher rates of glycolysis/nMol ATP compared to the high MP cells (n = 3).

(E) Determination of cellular source of NADH: flow cytometry profiles of high (upper) and low (lower) MP cells before (left) and after (right) treatment with antimycin A (AMA). Note the significant shift of most of the high MP cells after AMA treatment (upper right panel) and the minimal shift of low MP cells in response to AMA (lower right panel). The bar graph shows quantification of the percentage of cells with increased NADH fluorescence in response to AMA (n = 3). This indicates that the majority of NADH in the low MP cells is derived from nonmitochondrial source(s). Data presented as mean ± SEM.

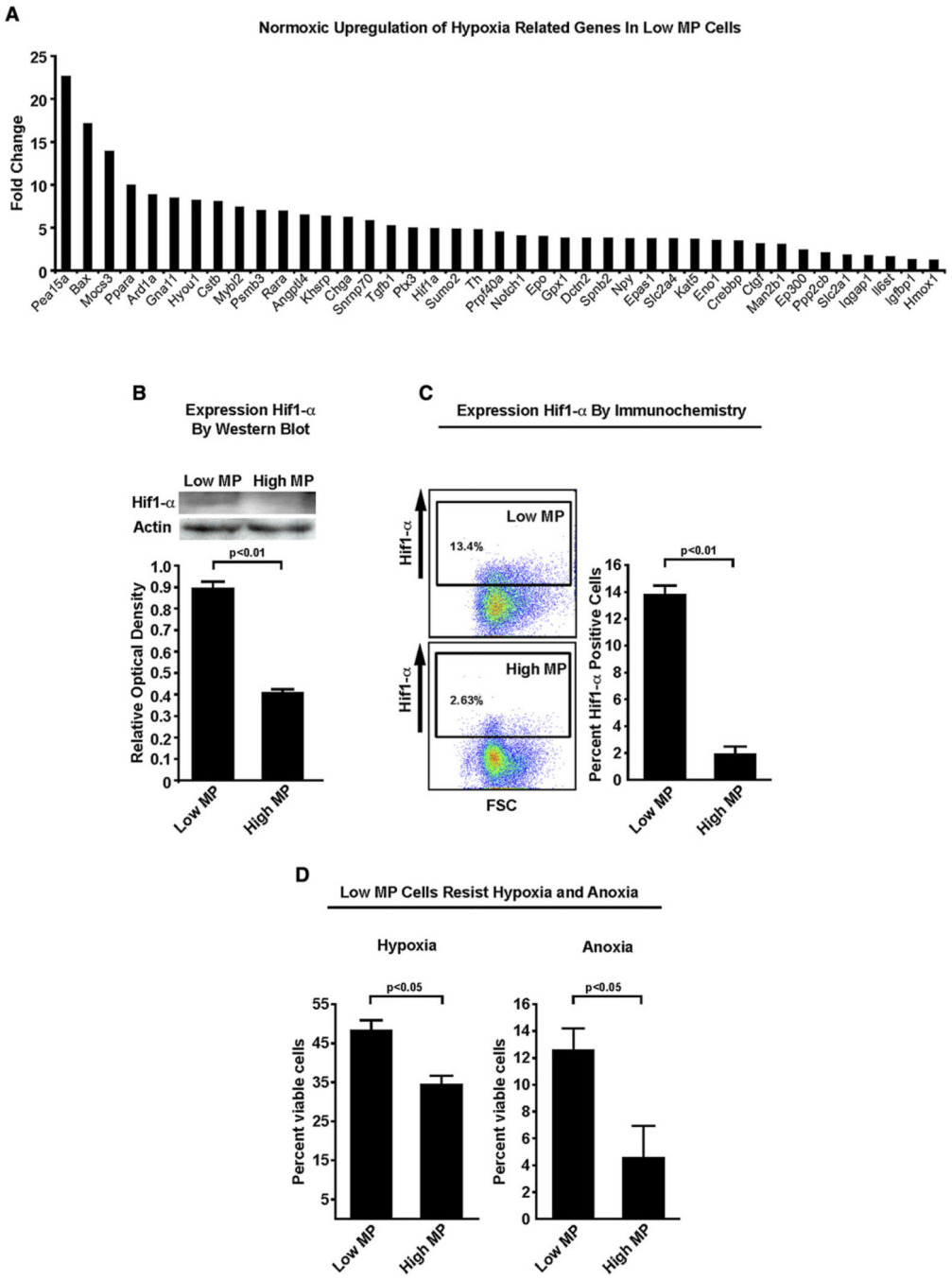

Figure 3. Normoxic Upregulation of Hif-1α in Low MP Cells

(A) Hypoxia real-time PCR array profile of low MP cells compared to high MP cells. Note the significant normoxic upregulation of hypoxia inducible genes in low MP cells under normoxic conditions (5–6 hr after isolation).

(B) Upper panel(s) show western blot analysis of high and low MP cells with Hif-1α antibody and actin as loading control. The lower panel shows densitometry analysis demonstrating higher Hif-1α protein expression in the low MP cells (n = 3).

(C) Immunocytochemistry staining demonstrating a higher percentage of low MP cells expressing Hif-1α compared to high MP cells (n = 3).
(D) Viability of low and high MP cells followed low-oxygen stress. The left panel shows the percentage of viable low and high MP cells after 12 hr of severe (1%) hypoxia. The right panel shows the percentage of viable low and high MP cells after 12 hr of anoxia (n = 3). Viability was assessed with trypan blue. Note the significantly higher viability in the low MP population after both hypoxia and anoxia. Data presented as mean ± SEM.
See also Figure S2.

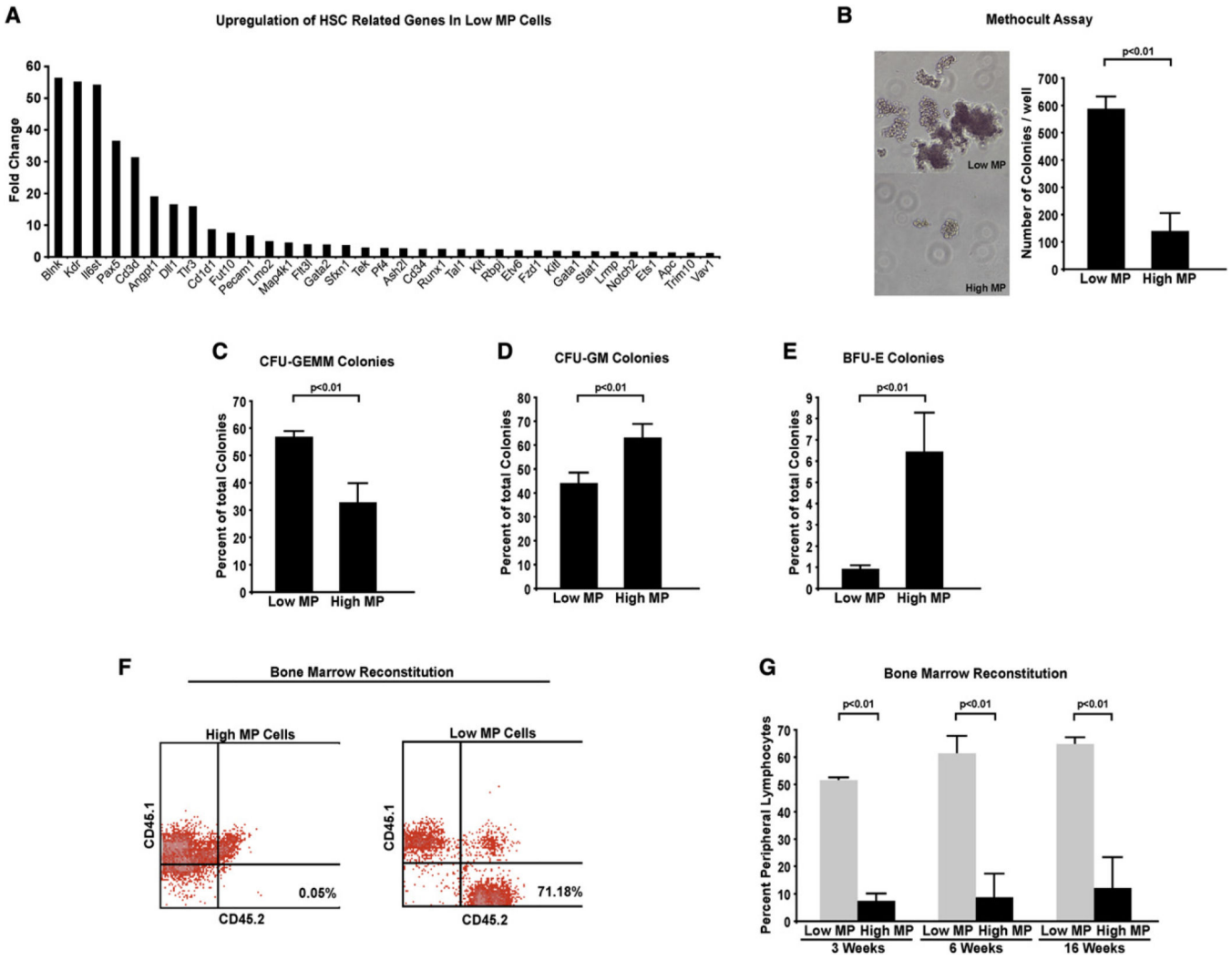

Figure 4. Low MP Cells Are Enriched for HSCs

(A) PCR array profile of low MP cells compared to high MP cells demonstrating enrichment of a number of HSCs associated genes in the low MP population.

(B) The left panel shows a representative bright field microscopic image of colonies obtained from low and high MP cells. The right panel shows quantification of colonies derived from low and high MP cells in methocult after 12 days.

(C) GFU-GEMM colonies.

(D) CFU-GM colonies.

(E) BFU-E colonies (n = 3). Note the significantly higher number of colonies derived from the low MP population. These results indicate that the low MP population is markedly enriched for hematopoietic progenitor cells.

(F) Representative flow cytometry profiles of peripheral blood of bone marrow recipient mice after staining with anti-CD45.2-FITC antibody (x axis) and anti-CD45.1-PE antibody (y axis), demonstrating higher engraftment in the recipient of low MP cells.

(G) Time course analysis of bone marrow reconstitution with low and high MP cells (n = 5 animals/group). Note the significantly higher bone marrow repopulation capacity of the low

MP cells at all time points. This result indicates that the low MP population is enriched for long term repopulating HSCs. Data presented as mean ± SEM.
See also Figure S1.

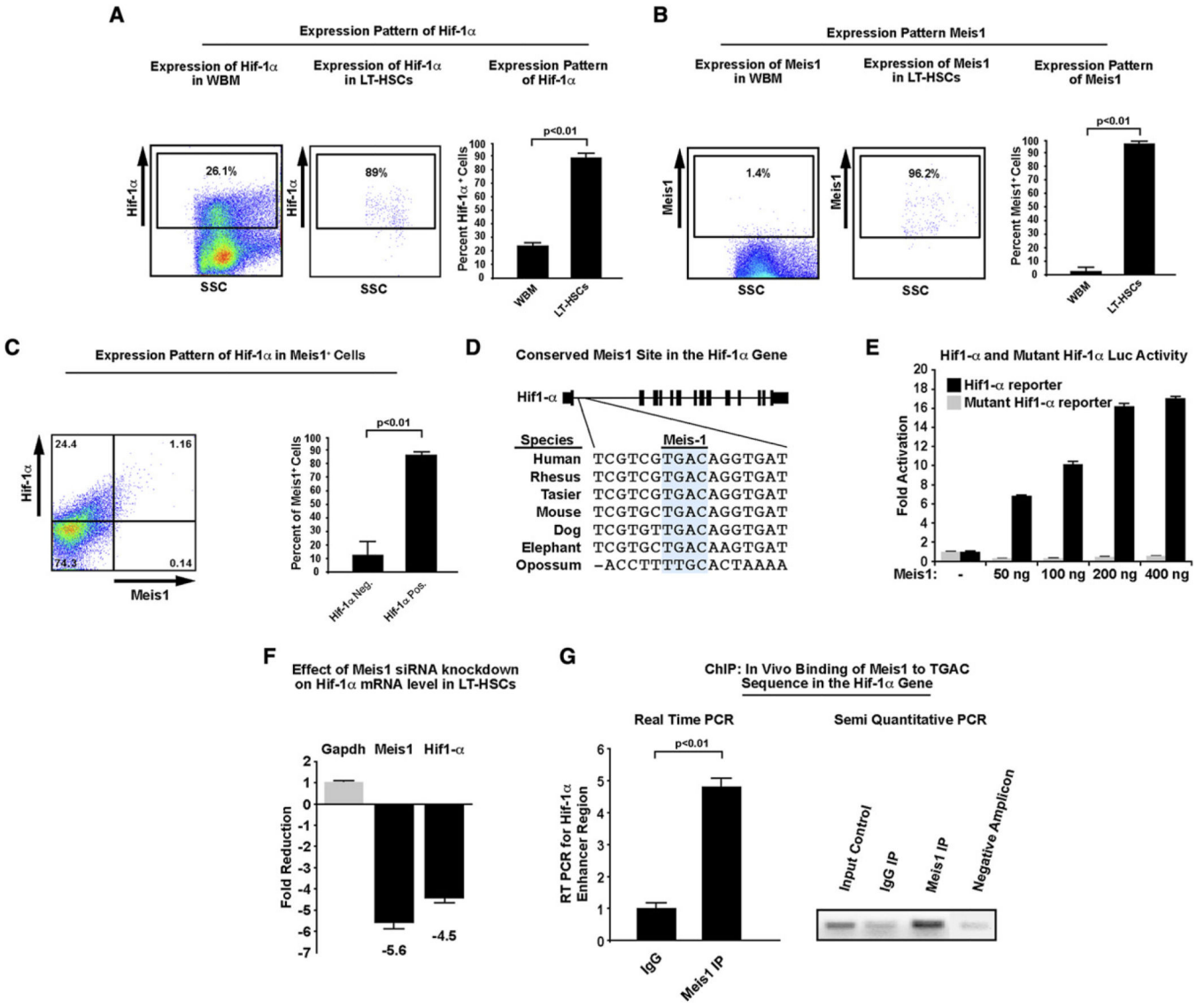

Figure 5. Transcriptional Regulation of *Hif-1α* by Meis1

(A) Expression pattern of Hif-1α. The left panel shows expression of Hif-1α in WBC. The middle panel shows expression of Hif-1α in LT-HSCs. The right panel shows quantification of Hif-1α expression. Note that whereas less than 25% of the unfractionated bone marrow cells express Hif-1α, the vast majority of LT-HSCs express Hif-1α protein (n = 3).

(B) Expression pattern of Meis1. The left panel shows expression of Meis1 in WBM. The middle panel shows expression of Meis1 in LT-HSCs. The right panel shows quantification of Meis1 expression. Note that whereas less than 2% of the unfractionated bone marrow cells express Meis1, almost all the LT-HSCs express Meis1 protein (n = 3).

(C) Colocalization of Hif-1α and Meis1 in the WBM. The left panel shows a representative flow cytometry profile of the expression of Hif-1α and Meis1. The right panel shows quantification of Hif-1α and Meis1 expression. Note that although only a small percentage of WBM cells express Meis1, the majority of these Meis1^{+} cells also coexpress Hif-1α (n = 3).

(D) Schematic of the conserved Meis1 binding domain in the first intronic region *Hif-1*α.
(E) Luciferase assay demonstrating dose dependent increase in *Hif-1*α luciferase activity after transfection with Meis1 expression vector. Mutation of the four nucleotides *Meis1* seed region completely abolishes the luciferase activity (n = 3).
(F) Real-time PCR following siRNA knockdown of *Meis1* in freshly isolated LT-HSCs. Knockdown of *Meis1* in LT-HSCs (5.6-fold) resulted in marked downregulation of *Hif-1*α mRNA levels (4.5-fold), (n = 3).
(G) ChIP assay demonstrating in vivo binding of Meis1 to its consensus binding sequence in the *Hif1*-α first intron. The left panel shows real-time PCR with primers flanking the consensus Meis1 binding sequence compared to control IgG after immunoprecipitation. The right panel shows PCR products showing input control and negative amplicon (n = 3). Data presented as mean ± SEM.
See also Figure S2.